Title

Targeting the αVβ3/NgR2 pathway in neuroendocrine prostate cancer.

Authors

Testa, Anna

Quaglia, Fabio

Naranjo, Nicole

et al.

Publication Date

2023-12-01

DOI

10.1016/j.matbio.2023.11.003

Peer reviewed

HHS Public Access

Author manuscript

Matrix Biol. Author manuscript; available in PMC 2024 January 29.

Published in final edited form as:

Matrix Biol. 2023 December ; 124: 49–62. doi:10.1016/j.matbio.2023.11.003.

Targeting the αVβ3/NgR2 pathway in neuroendocrine prostate cancer

Anna Testa[a,b,1], **Fabio Quaglia**[a,b,1], **Nicole M. Naranjo**[a,b], **Cecilia E. Verrillo**[a,b], **Christopher D. Shields**[a,b], **Stephen Lin**[a,b], **Maxwell W. Pickles**[a,b], **Drini F. Hamza**[a,b], **Tami Von Schalscha**[c], **David A. Cheresh**[c], **Benjamin Leiby**[d], **Qin Liu**[e], **Jianyi Ding**[e], **William K. Kelly**[f], **D. Craig Hooper**[a,b], **Eva Corey**[g], **Edward F. Plow**[h], **Dario C. Altieri**[i], **Lucia R. Languino**[a,b,*]

[a]Prostate Cancer Discovery and Development Program, Thomas Jefferson University, Philadelphia, PA, United States

[b]Department of Pharmacology, Physiology, and Cancer Biology, Thomas Jefferson University, Philadelphia, PA, United States

[c]Department of Pathology, Moores Cancer Center, and Sanford Consortium for Regenerative Medicine, University of California San Diego, La Jolla, CA, United States

[d]Division of Biostatistics, Department of Pharmacology, Physiology, and Cancer Biology, Sidney Kimmel Medical College, Thomas Jefferson University, Philadelphia, PA, United States

[e]Molecular and Cellular Oncogenesis Program, The Wistar Institute, Philadelphia, PA, United States

[f]Department of Medical Oncology, Thomas Jefferson University, Philadelphia, PA, United States

[g]Department of Urology, University of Washington, Seattle, WA, United States

[h]Department of Cardiovascular and Metabolic Sciences, Lerner Research Institute, Cleveland Clinic, Cleveland, OH, United States

[i]Immunology, Microenvironment and Metastasis Program, The Wistar Institute, Philadelphia, PA, United States

Abstract

Highly aggressive, metastatic, neuroendocrine prostate cancer, which typically develops from prostate cancer cells acquiring resistance to androgen deprivation therapy, is associated with limited treatment options and hence poor prognosis. We have previously demonstrated that the αVβ3 integrin is over-expressed in neuroendocrine prostate cancer. We now show that

*Corresponding author at: Thomas Jefferson University, Philadelphia, PA, United States.
[1]Anna Testa and Fabio Quaglia, co-first authors.

Declaration of Competing Interest

FQ is an employee/contractor at Janssen Pharmaceutical. EC is a consultant of Dotquant and received funding under institutional SRA from Janssen Research, Bayer Pharmaceuticals, Forma Therapeutics, Foghorn, Kronos Bios, Genentech, Astra Zeneca, and MacroGenics. No potential conflict of interest was reported by the other authors.

Supplementary materials

Supplementary material associated with this article can be found, in the online version, at doi:10.1016/j.matbio.2023.11.003.

LM609, a monoclonal antibody that specifically targets the human αVβ3 integrin, hinders the growth of neuroendocrine prostate cancer patient-derived xenografts *in vivo*. Our group has recently identified a novel αVβ3 integrin binding partner, NgR2, responsible for regulating the expression of neuroendocrine markers and for inducing neuroendocrine differentiation in prostate cancer cells. Through *in vitro* functional assays, we here demonstrate that NgR2 is crucial in promoting cell adhesion to αVβ3 ligands. Moreover, we describe for the first time co-fractionation of αVβ3 integrin and NgR2 in small extracellular vesicles derived from metastatic prostate cancer patients' plasma. These prostate cancer patient-derived small extracellular vesicles have a functional impact on human monocytes, increasing their adhesion to fibronectin. The monocytes incubated with small extracellular vesicles do not show an associated change in conventional polarization marker expression and appear to be in an early stage that may be defined as "adhesion competent". Overall, these findings allow us to better understand integrin-directed signaling and cell-cell communication during cancer progression. Furthermore, our results pave the way for new diagnostic and therapeutic perspectives for patients affected by neuroendocrine prostate cancer.

Keywords

Neuroendocrine prostate cancer; αVβ3 integrin; NgR2; Patient plasma; Small extracellular vesicles; Monocytes

Introduction

The αVβ3 integrin belongs to a group of transmembrane receptors composed of two subunits, α and β, involved in adhesion processes between cells and the extracellular matrix (ECM). Integrins often show an altered expression in numerous types of cancer, including prostate cancer (PrCa) [1]. In particular, αVβ3, weakly detectable in normal prostate cells, is expressed at high levels in advanced PrCa. This integrin is also known to protect disseminated tumor cells from chemotherapy and to promote cancer cell invasion and adhesion to ECM proteins [2,3]. Moreover, it is highly expressed in metastasis, where the αVβ3 integrin acts as a critical component in the metastatic process [4]. Given these implications, the αVβ3 integrin has been suggested as a potential target in several cancers [5,6]. However, the αVβ3 integrin had not been analyzed in the most aggressive forms of PrCa before our previous publications [7,8]. Through a series of investigations based on *in vitro* methods and *ex vivo* analyses of patient-derived xenografts (PDXs), human neuroendocrine prostate cancer (NEPrCa) specimens, and mouse models of NEPrCa, we have demonstrated that the αVβ3 integrin is highly expressed in human and mouse models of NEPrCa. In contrast, it is absent in prostate adenocarcinoma (ADPrCa) [7,8].

NEPrCa is an aggressive and metastatic subtype of PrCa, associated with extremely poor prognosis [9,10]. It generally develops from subsets of cells that acquire genetic alterations in response to multiple lines of androgen-deprivation treatment [11,12]. The less frequent *de novo* NEPrCa arises when mature differentiated prostate cells acquire androgen receptor (AR)-independent pro-tumorigenic mutations [13]. As a result, these cells exhibit poor or no expression of AR or prostate-specific antigen (PSA) and are characterized by expression of neuron-specific markers, such as synaptophysin (SYP), chromogranin A (CHGA), and

neuron-specific enolase (NSE) [9,11,14]. In contrast, some forms of NEPrCa that arise in response to therapies, although generally similar to *de novo* NEPrCa, preserve AR expression [15]. This classification is continuously being revisited as new findings indicate that the double-negative (AR-null; NE-null) PrCa incidence is growing [16]. Therefore, there is a need for new therapeutic strategies for NEPrCa.

Many studies, including our investigations, have shown that extracellular vesicles (EVs) have an important role in intercellular communication, both in malignancies and other diseases [7,17–25]. Small EVs (sEVs) are 50–150 nm vesicles detectable in various biologic fluids, such as blood, interstitial fluid, urine, and medium of cultured cells [25,26]. Not only are sEVs very abundant in human blood (10^9–10^{10}/mL), but also specific subtypes have been shown to be upregulated in cancer [27]. Hence, the interest generated around the sEV research has grown in the last decade. The presence of tumor-derived sEVs in the plasma of patients affected by several types of cancer has been related to advanced disease stages [28]. We and others have also demonstrated that sEVs released from cancer cells promote reprogramming of recipient cells, inducing an aggressive phenotype [7,29,30]. Moreover, studies have described the role of integrins expressed by tumor-derived sEVs in mediating organ-specific metastasis tropism [17]. Thus, targeting sEV biogenesis and release has clinical implications for PrCa therapy [31].

We have recently shown that the expression of the αVβ3 integrin, which is highly expressed in human sEVs, increases the levels of NgR2 (Nogo-66 receptor homolog 1) [32,33] in PrCa cells [34]. We also demonstrated that NgR2 induces neuroendocrine differentiation (NED) in recipient cells [34]. NgR2 belongs to the Nogo receptor family, which includes NgR1 and NgR3; these structurally related molecules are glycosylphosphatidylinositol (GPI)-anchored receptors, lacking both the transmembrane and the intracellular domains [32,33]. NgR1 and NgR2 are receptors for myelin associated glycoprotein (MAG), which binds NgR2 with greater affinity than NgR1 [33,35,36]. The bond between members of the NgR family and MAG triggers a signal transduction complex activating several downstream pathways [32,37–39], mainly associated with neuronal growth [40]. Multiple datasets, analyzed in Quaglia et al. [34] show increased levels of RTN4RL2 (the gene encoding NgR2) RNA in advanced PrCa tumors; however, the role of NgR2 has been examined predominantly in neuroscience studies, minimally in cancer, and never in EVs.

The cross-talk between cancer cells and tumor microenvironment (TME) components, such as immune cells, fibroblasts, and endothelial cells, is well established [41,42]. In particular, tumor-associated macrophages (TAMs), derived from resident macrophages and newly recruited monocytes, represent the major constituents of the TME [43, 44]. Two phenotypes of TAMs are commonly recognized: classically activated M1 and alternatively activated M2. M1 are pro-inflammatory and anti-tumoral, and are characterized by the surface expression of CD80, CD86, and HLA-DR. M2 exert an immunosuppressive and pro-tumorigenic activity, and their main surface markers are CD206, CD163, and CD204 [42,44–46]. Although this dichotomy has been acknowledged as an over-simplification, an imbalance between M1 and M2 in favor of M2 in the TME, appears to be associated with tumor growth, angiogenesis, and metastasis [42,47,48]. sEVs have been recognized not only as important mediators of communication among the various components of the TME [41],

but also, when isolated from numerous cancer cell lines [49], including prostate [50–52], as modulators of macrophage polarization *in vitro*. However, the effect of PrCa patient-derived sEVs on human macrophages has yet to be assessed and could provide better understanding of the complex cell-cell communication in the TME.

Our study, via *in vivo* murine models and *in vitro* assays based on PrCa patients and healthy donor samples, as well as cell lines, provides new understanding of integrin-mediated mechanisms behind NEPrCa progression and new therapeutic strategies to treat it.

Results

LM609, a monoclonal antibody to the αVβ3 integrin, inhibits NEPrCa-PDX tumor growth in vivo

Based on our previous finding that the αVβ3 integrin is selectively upregulated in NEPrCa [8], we hypothesized that its inhibition in NEPrCa-PDXs would negatively impact NEPrCa growth. In the experiments shown here, we targeted the αVβ3 integrin in PDXs using LM609, a monoclonal antibody (mAb) specific to the human αVβ3 [53–56].

As shown in Supplementary Fig. 1 A, we purified LM609 from ascites using a chromatography column packed with Protein-A Sepharose beads. We then characterized it *in vitro*, showing that our preparations are free of contaminants (Supplementary Fig. 1 B). The adhesion assay depicted in Supplementary Fig. 1 C demonstrates that LM609 actively inhibits the adhesion of PC3 cells to fibrinogen in a concentration-dependent manner.

Then, we tested the effect of LM609 on two NEPrCa PDXs (LuCaP 145.2 and LuCaP 173.1) that we have shown to express high levels of αVβ3 and have NE characteristics [8] (Fig. 1). LuCaP 145.2 tumor bits were subcutaneously implanted in 6–8-week-old CB-17 severe combined immunodeficient (SCID) male mice ($n = 15$); the same experiment was repeated with LuCaP 173.1 ($n = 15$) [57]. Once tumors reached a volume of ~ 100–150 mm^3, mice were treated with either LM609, IgG1 as non-immune control, or phosphate-buffered saline (PBS). For all mice, trends of the xenograft volumes over time were registered by measuring them twice a week, starting from the first day of treatment (Fig. 1A–B). After three weeks, mice in each group were euthanized. As shown in Fig. 1, treatment with LM609 significantly reduces tumor growth.

As presented in Tables 1–4, the inhibition of the αVβ3 integrin, using the LM609 mAb, decreases NEPrCa LuCaP 145.2 and LuCaP 173.1 tumor volumes. Statistically significant differences are observed between LM609 and the other groups for both LuCaP 145.2 and LuCaP 173.1 (Tables 2 and 4).

NgR2 expression increases cell adhesion to αVβ3 ligands

We have previously shown that high levels of αVβ3 increase the expression of NgR2, a novel αVβ3 binding partner and NE marker regulator in PrCa cells [34]. To further investigate whether NgR2 affects cell attachment to αVβ3 ligands, we used adhesion assays [34]. First, we tested the expression of the following epitopes of αVβ3: LIBS1, 2 and 6. The immunoblotting (IB) analysis depicted in Supplementary Fig. 2 provides evidence

that LIBS2 or the AP5 epitopes are not detected in DU145 NgR2 and Mock transfectant cell lines; in addition, although minimally expressed, there are no differences in the αVβ3 expression of LIBS1 and 6 epitopes (data not shown).

Then, we performed adhesion assays using two different cell populations of DU145 transfectants that express NgR2 (DU145 NgR2) and two different cell populations of Mock controls not expressing NgR2 (DU145 Mock) (Fig. 2A–D). DU145 NgR2 cells and DU145 Mock cells were seeded for 1 h on fibrinogen, vitronectin, collagen, laminin, or bovine serum albumin (BSA) coated wells. The results show that DU145 NgR2 cells bind to fibrinogen and vitronectin, αVβ3 ligands, significantly more than Mock controls. To confirm that this adhesion depends on αVβ3, we seeded DU145 NgR2 cells on fibrinogen, laminin or BSA coated wells; prior to the addition of cells, wells were incubated with either LM609 [10 μg/mL (data not shown) or 20 μg/mL], IgG1 as non-immune control [10 μg/mL (data not shown) or 20 μg/mL] or left untreated (Fig. 2E). These data show that LM609 significantly inhibits DU145 NgR2 cells to fibrinogen but not to laminin. These results demonstrate that αVβ3 is found in an “adhesion competent” state, but not LIBS-dependent, on the basis of its interaction with NgR2. The results also indicate that the effect of NgR2 is specific for αVβ3, since cell adhesion to collagen and laminin is not affected (Fig. 2C–E). Overall, these results demonstrates that NgR2 is critical for cell adhesion to αVβ3 ligands.

The αVβ3 integrin and NgR2 in prostate cancer patient plasma-derived small extracellular vesicles

We have previously demonstrated that the αVβ3 integrin and its binding partner NgR2 are highly expressed in NEPrCa [8]. We also showed that PrCa cell-derived sEVs are enriched in αVβ3, which is barely detectable in healthy donor sEVs [58] and induce NED in recipient cells [7].

We isolated sEVs from plasma via ultracentrifugation, followed by iodixanol density gradient (IDG) ultracentrifugation (Fig. 3A). The sEVs were then characterized by IB (Fig. 3B–C) and shown to express sEV markers such as CD9 and Syntenin.

We have previously shown that PrCa patient-derived sEVs express αVβ3 [58]. We tested if these circulating sEVs express NgR2 as well, and to answer this question we performed an IB analysis of pooled sEVs isolated from metastatic PrCa patients. As shown in Fig. 4A, we demonstrate for the first time that NgR2 is expressed in sEVs isolated from the plasma of PrCa patients. To better investigate the association of αVβ3 and NgR2 in PrCa patient-derived sEVs, we performed an IB analysis of density gradient-isolated fractions. Fig. 4B–C show that the sEV markers TSG101, Syntenin, and CD9 are detected in the same fractions that express αVβ3 and NgR2. Patient G (Fig. 4B) shows a partial co-sedimentation of αVβ3 and NgR2, which is fully detected in patient H (Fig. 4C). Therefore, our data establish for the first time that, although at different degrees, αVβ3/NgR2 co-fractionate in PrCa patient circulating sEVs.

Fractions six to eight, corresponding to density values ranging from 1.12 to 1.19 g/mL, were pooled and analyzed using nanoparticle tracking analysis (NTA); the results show that these vesicles fall into the expected sEV size range of 50–150 nm [26] (Fig. 5).

Overall, these results demonstrate that the αVβ3 integrin and NgR2 are expressed in circulating sEVs in metastatic PrCa patients.

Adhesion of monocytes to fibronectin increases after incubation with sEVs derived from PrCa patients in a NgR2-dependent manner

Many studies have demonstrated that TAMs derived from resident macrophages and newly-recruited monocytes represent the major constituents of the TME [43,44] and that sEVs released by cancer cells play a role in the communication with immune cells in the TME [52].

We hypothesized that PrCa plasma derived-sEVs, enriched in αVβ3 and NgR2, could affect monocyte activity. To test this, we isolated peripheral blood mononuclear cells (PBMCs) from healthy volunteers and incubated them with sEVs isolated from either healthy donors or PrCa patients; PBS-treated cells were used as a control. PBMCs were incubated with sEVs isolated from different healthy individuals. Forty-eight hours after treatment, monocytes attached to wells were isolated and adhesion assays performed. As shown in Fig. 6A–D, treatment with PrCa patient-derived sEVs significantly increases the adhesion of monocytes to fibronectin (FN). In two out of four experiments (Fig. 6A–B), no significant difference in cell adhesion was observed between untreated and healthy donor sEV-treated cells. In three out of four cases, untreated monocytes adhered to FN more than to BSA; in three out of four cases, monocytes incubated with healthy donor-derived sEVs adhered to FN more than to BSA; in all the experiments, monocytes incubated with PrCa patient-derived sEVs adhered to FN more than to BSA. However, pre-incubation of PrCa patient-derived sEVs with LM609 did not impact the adhesion to FN compared to either non-immune IgG or no sEV pre-treatment (Supplementary Fig. 3). This is consistent with our previous findings, suggesting that the uptake of sEVs is not mediated by the presence of αVβ3 on the cell surface [7].

Our adhesion assays confirm that sEVs from PrCa patient plasma have a functional impact on monocyte activity *in vitro* and may promote monocyte infiltration known to occur in PrCa as shown in Supplementary Fig. 4.

To further confirm the role of NgR2 in monocyte functional activity, PBMCs isolated from healthy volunteers were plated and incubated with sEVs isolated from PC3 cells transfected with two shRNA constructs that target RTN4RL2 (shRTN4RL2_1 and shRTN4RL2_2) or with a non-targeting scrambled control shRNA (ShScramble). Untreated cells were used as a control. Forty-eight hours after treatment, monocytes attached to wells were isolated and adhesion assays were performed. As shown in Fig. 7A–B, treatment with sEVs released from cells expressing NgR2 significantly increases the adhesion of monocytes to fibronectin compared to cells in which NgR2 is silenced. Fig. 7C demonstrates that the sEVs released from these cells fall into the expected sEV size range of 50–150 nm [26]. This demonstrates that the sEV-dependent functional impact on monocyte activity *in vitro* relies upon NgR2 expression.

The expression of M1 and M2 markers in monocytes isolated from healthy volunteers is not affected by sEVs derived from PrCa patients

Given that sEVs play a role in the inter-communication between cancer cells and immune cells, we investigated whether treatment with PrCa patient plasma-derived sEVs could lead to a phenotypic change in healthy volunteer monocytes. PBMCs from healthy volunteers were incubated with either PBS (control) or PrCa patient sEVs for 48 h. Flow cytometric analysis for CD14, a monocyte/macrophage marker [59], was used to gate monocytes among PBMCs. Subsequently, CD14+ cells were evaluated for the surface expression of CD163 and CD204, markers associated with M2 polarization or CD80 and HLA-DR, associated with M1 polarization. As shown in Fig. 8A–B, PrCa patient-derived sEVs do not affect M2 or M1 marker expression. As additional control, in another set of experiments, PBMCs were subjected to incubation with PBS, healthy donor-derived sEVs or PrCa patient-derived sEVs. As shown in Fig. 8C–D, neither sEVs isolated from healthy donors nor sEVs isolated from PrCa patients have an impact on M2 or M1 marker expression.

Overall, these results suggest that the functional effect exerted by sEVs on monocytes does not correlate with a phenotypical alteration.

Discussion

We demonstrate in this paper that a mAb targeting specifically the αVβ3 integrin is highly effective in reducing NE prostate tumor growth *in vivo*. We also provide evidence that NgR2, an αVβ3 binding partner, which is upregulated in NEPrCa, is crucial for αVβ3 adhesion to its ligands. Finally, we show that both αVβ3 and NgR2 are detectable in patient plasma-derived sEVs and that these sEVs functionally impact monocyte activity *in vitro*.

Our results demonstrate a significant reduction of NE tumor growth upon treatment with LM609 and propose this therapeutic approach for NEPrCa patients. The molecular basis of the interaction between LM609 and αVβ3, has yet to be fully clarified. Two mechanisms of action have been hypothesized: an Arg-Gly-Asp (RGD)-dependent manner [60,61] and one that does not involve the RGD-binding pocket occlusion based on a sterical hindering of the RGD ligand binding [55]. A possible limitation of RGD-based anti-αVβ3 drugs could be the difficulty of overcoming the high interstitial tumor pressure, crossing the vascular wall and penetrating the tumor parenchima [62,63]. This does not seem to affect the results in our murine model.

Various αVβ3 activation states corresponding to different conformations have been reported, acknowledging that, when bent, the ligand affinity is low and αVβ3 is inactive, whilst the extended form results in “adhesion competent” high-affinity ligand binding [64–66]. Among others, LIBS epitopes have been shown in the αVβ3 active form [67]. However they were not affected by NgR2 expression in our analysis, although our functional assays show no interaction between αVβ3 and its ligands in the absence of NgR2. This effect may result in increased migration and infiltration in the tumor, or like for Tcells [68], may just facilitate these cells’ trapping in the prostate TME for local control of the immune response. We therefore suggest that NgR2 is involved in an αVβ3 conformational change leading

to its activation state and that this NgR2/active αVβ3 complex may have a role in PrCa reprogramming towards a NE phenotype.

Although multiple datasets show increased levels of RTN4RL2 (the gene encoding NgR2) RNA in advanced PrCa patients [34], the role of NgR2 in NE cancer progression was not explored before our paper was published [34] and had never been analyzed in sEVs. Because NEPrCa is characterized by late diagnosis, based on metastatic biopsy in patients with spread aggressive disease with low or absent PSA levels [69], NgR2 may represent a promising, specific marker for a non-invasive diagnosis.

The role of TME in tumor growth, invasion, and progression is well established [42,45,46], making its components an interesting target of studies for diagnostic and therapeutic purposes. However, more investigations are needed to deeply understand how cancer cells affect monocytes/macrophages to promote cancer progression. Several studies have described an effect of cancer cell line-derived EVs and sEVs on macrophages *in vitro* [49–51,70]. Here, we demonstrate that PrCa patient plasma-derived sEVs increase monocyte adhesion. These sEV-incubated, more adherent monocytes do not show altered expression of the polarization markers tested, seemingly in a state that may be defined as “highly adhesive without alterations of conventional polarization markers”. We can hypothesize a model where PrCa cells release sEVs enriched in αVβ3 and NgR2, thereby increasing TAM accumulation. This aligns with previous findings, assessing that αVβ3 in epithelial cancers positively correlates with tumor growth-associated macrophages [54].

In a recent study, an increase of M2 markers after treatment with healthy volunteer plasma-derived sEVs was achieved after co-stimulating the monocytes with macrophage colony-stimulating factor [71]. Both treatment with MCSF and exposure to the toll-like receptor agonists were required to obtain a larger release of TNF-α, a M1-associated cytokine [71]. Thus, significant modifications in the expression of M1 and M2 markers after treatment with patient or healthy donor sEVs may occur in more complex steps dependent upon stimulating co-factors.

We conclude that sEVs enriched in the αVβ3/NgR2 complex, may have a causal role in promoting a metastatic phenotype, maintaining αVβ3 in an adhesion competent state, and affecting immune and other cells in the TME. The results presented here enable us to reach a comprehensive mechanistic understanding of integrin-directed signaling and cell-cell communication during NEPrCa progression and will open new possibilities in future studies for the design of NgR2-based therapeutic and diagnostic strategies of PrCa patients.

Materials and methods

Antibodies

The following primary antibodies (Abs) were used for IB analysis: goat polyclonal Ab against NgR2 (R&D System, AF2776), mouse monoclonal Ab against CD9 (Santa Cruz, sc13118), LIBS1 [72], LIBS2 (Millipore, MABT27), Ab33/LIBS6 (ascites) [72] and AP5 (Kerafast, [73]); rabbit monoclonal Abs against β3 (Cell Signaling, 13166S) and Syntenin (Abcam, ab133267), rabbit polyclonal Abs against TSG101 (ab30871, Abcam), Calnexin

(24,335, Cell Signaling) and β3 (serum) [23]. The following secondary Abs were used for IB analyses: HRP linked anti-goat IgG (R&D Systems), HRP-linked anti-mouse IgG (Cell Signaling, 7076 S) and HRP-linked anti-rabbit IgG (Cell Signaling, 7074 S).

The following Abs were used for the adhesion assays: mouse monoclonal against human αVβ3 integrin LM609 (MAB1976, Millipore) and non-immune mouse monoclonal IgG1 (BE0083, Bio X Cell).

The following Abs were used for IHC analysis: rabbit monoclonal Ab against F4/80 (70076S, Cell Signaling) and non-immune rabbit IgG (I5006, Sigma).

The following Abs were used for the PDX treatment: mouse monoclonal IgG1 LM609 [61] and non-immune mouse monoclonal IgG1 (BE0083, Bio X Cell).

Flow cytometry experiments were conducted using the following mouse Abs to human: Alexa Fluor 488 conjugated CD14 (BD Biosciences, 562,689); for M2 polarization phenotyping: APC-conjugated CD163 (Miltenyi, 130–112–129 or Biolegend, 333,610), PE conjugated CD204 (BD Biosciences, 566,251); for M1 polarization phenotyping: APC conjugated CD80 (Biolegend, 305,220), PE-conjugated HLA-DR (BD Biosciences, 555,812); for isotype control: Alexa Fluor 488 conjugated IgG2b,κ isotype control (BD Biosciences, 558,716), APC conjugated REA control antibody IgG1, REAfinity™ (Miltenyi, 130–113–446) or APC conjugated IgG1,κ isotype control antibody (Biolegend, 400,120) and PE conjugated IgG1,κ isotype control (BD Biosciences, 551,436).

Cell lines

PrCa cell lines (DU145 and PC3) were cultured as previously described [24,58]. DU145 cells were transfected with pCMV6-Entry vector carrying RTN4RL2 (DU145 NgR2 cells) (Origene, SC310413) or an empty vector (DU145 Mock cells) (Origene, PS100001) as previously described [34]. Transfected cells were maintained using 0.5 mg/mL G418. When transfectants were generated, PC3 cells were transfected with two different shRNA constructs that target RTN4RL2 (SMARTvector, Dharmacon/Horizon, SO-2,914,049 G, sequences: V3SVHS00_4,716,901 for shRTN4RL2_1 and V3SVHS00_7,164,907 for shRTN4RL2_2). As a control, PC3 cells were transfected with a non-targeting scrambled control shRNA (SMARTvector, Dharmacon/Horizon, VSC11707), as previously described [34].

LM609 purification

LM609 purification was performed as previously described [61]. Briefly, LM609 ascites was cleaned with Cleanascite (Fisher, NC0542680C), diluted in a sodium chloride and glycine binding buffer, and recirculated over a Protein A column. The column was washed and the Ab was eluted with elution buffer (0.1 M Citric Acid, pH 6). Fractions of 500 μL were collected and the O.D. at 280 nm was measured using a NanoDrop 2000c spectrophotometer. Purified peak fractions with OD280 greater than 0.1 containing the Ab were pooled together. Afterwards, they were dialyzed in PBS and concentrated. Finally, the Ab was run through SDS-PAGE to confirm purity (Supplementary Fig. 1).

PDX expansion, re-implantation and mouse treatment

LuCaP 145.2 and LuCaP 173.1 PDXs were provided by the University of Washington, where they were acquired, established and characterized as previously described [57]. To expand the PDXs, thawed ~5–10 mm^3 tissue bits were subcutaneously implanted in a first group of SCID CB-17 mice (Charles River) according to the National Cancer Institute 2017 SOP guidelines. One drop of Matrigel (356,237, Corning) was added to each bit before injection by trocar. Mice carrying tumors of ~500 mm^3 were euthanized; these tumors were harvested and stepped-rate cryopreserved as previously described [57]. Volumes were calculated following the formula reported below.

After thawing, ~5–10 mm^3 tumor bits were subcutaneously implanted in the axillary area of a second group of 30 SCID CB-17 mice (LuCaP 145.2, n =15; LuCaP 173.1, n = 15), as described in the National Cancer Institute 2017 SOP guidelines. Mice were monitored twice a week for tumor growth. Once the tumors reached a volume of ~100–150 mm^3, the treatment was started. The treatment groups were: LM609 10 mg/kg (LuCaP 145.2, n = 5; LuCaP 173.1, n = 5); mouse monoclonal IgG1 10 mg/kg (LuCaP 145.2, n = 5; LuCaP 173.1, n = 5) and PBS (LuCaP 145.2, n = 5; LuCaP 173.1, n = 5). Treatment was administered intraperitoneally twice weekly for three weeks and during this period, volumes were measured twice a week. After 21 days, mice were euthanized and tumor volume measured according to the formula reported below:

$$\text{Tumor volume(mm3)} = \frac{(tumor\ lenght) \times (tumor\ \ width)^2}{2}$$

Animal care

SCID CB-17 mice—SCID CB-17 male mice (Charles River) were cared for and monitored according to the Office of Laboratory Animal Welfare, NIH, and Department of Health and Human Services standards. Thirty SCID mice were used; no female mice were analyzed in this study. Institutional Animal Care and Use Committee recommendations were followed, and the protocol was approved by the Institutional Animal Care and Use Committee at Thomas Jefferson University (protocol number: 04–499).

Transgenic adenocarcinoma of the mouse prostate mice—Transgenic Adenocarcinoma of the Mouse Prostate (TRAMP) male mice were generated as previously described [74]. Nine TRAMP mice and five WT mice were used; no female mice were analyzed in this study. Care of animals was in compliance with standards established by the Office of Laboratory Animal Welfare, NIH, and Department of Health and Human Services standards. Institutional Animal Care and Use Committee recommendations were followed, and the protocol was approved by the Institutional Animal Care and Use Committee at Thomas Jefferson University (protocol number: 1204).

Human subject inclusion criteria—Twenty-two PrCa patients' blood or plasma was obtained at Thomas Jefferson University (Philadelphia, PA) to isolate sEVs. Sixteen healthy volunteers' blood or plasma was obtained at Thomas Jefferson University (Philadelphia, PA) to isolate sEVs and/or isolate PBMCs. Specimens were de-identified and discarded

in accordance with guidelines established by the Institutional Review Board (IRB), an administrative body established to protect the rights and welfare of human subjects recruited to participate in research activities conducted at Thomas Jefferson University (protocol number: 19D.011).

EV isolation via ultracentrifugation—EV isolation by differential ultracentrifugation was performed as previously described [75].

sEV isolation via iodixanol density gradient ultracentrifugation—sEV isolation by IDG ultracentrifugation was performed as previously described [75].

Immunoblotting—IB analysis was performed as previously described [24,34,72].

Immunohistochemical analysis—IHC was performed as previously described [34].

Nanoparticle tracking analysis—NTA was performed as previously described [7]. Briefly, pooled iodixanol fractions were diluted 1:200 in PBS and analyzed using NanoSight NS300. Samples were infused using a syringe pump, with an infusion rate of 60 for consistent flow. Three 30 s videos were captured, with a standard measurement setting. Data were collected at 25 °C, with camera level ranging from 13 to 16 and screen gain ranging from 1 to 3. Detection threshold was set at 4 for plasma-derived sEVs and at 5 for cell-derived sEVs. Data analysis was performed using NTA software version 3.1.54.

PBMC isolation, culture, and EV treatment—Human blood was withdrawn via venipuncture, and coagulation was prevented by treatment with Acid Citrate Dextrose (ACD). Anti-coagulated blood was centrifuged at 100 × g for 20 min at room temperature with acceleration 1 and break 0 to separate plasma. The remaining blood was diluted with PBS in a 1:1 ratio. The mixture was layered over Ficoll-Paque (Cytvia,17,144,002) in a ratio of volume 2:1 and centrifuged at 2000 × *g* for 20 min at 4 °C with the break off to isolate the buffy coat. PBMCs were collected, washed with PBS, and pelleted via centrifugation at 1500 × *g* for 10 min at 4 °C. PBMCs were cultured in RPMI media supplemented with 10 % fetal bovine serum (FBS), 1 % penicillin/streptomycin, and 1 % of L-Glutamine on 6-well plates (1×10^6 cells/well). Within 24 h, PBMCs were treated with 1×10^9 sEVs derived from PrCa patient or healthy donor plasma for 48 h. For a second set of experiments, PBMCs were incubated with 1×10^9 sEVs, derived from PrCa patient plasma, that were previously incubated for 1 h prior to the treatment with LM609 10 μg/mL, non-immune IgG1 10 μg/mL, or PBS. For a third set of experiments, PBMCs were treated with 1×10^9 sEVs derived from PC3 cells transfected with one of the shRNA constructs that target RTN4RL2 (shRTN4RL2_1, or shRTN4RL2_2); as control, PC3 cells were transfected with a non-targeting scrambled control shRNA. After 48 h, PBMCs were collected and analyzed via flow cytometry or used for functional assays, as described below.

LM609 characterization in adhesion assays—Cell adhesion assays were performed as previously described [76]. Briefly, non-treated 96 well plates (25–103, Olympus) were coated with 200 μL of fibrinogen 15 μg/mL or 1 % heat denatured filtered BSA as control overnight at 4 °C. On the day of the assay, the coated wells were blocked with 1 % BSA

in PBS for 30 min at room temperature followed by one wash with PBS and two washes with adhesion buffer (serum-free media [SFM], 0.5 % BSA, 0.2 mM $MnCl_2$). Wells were pre-loaded with 100 μL of either increasing Ab concentrations (0.1,0.2,0.4,0.8,1.6 μg/mL) diluted in adhesion buffer, adhesion buffer alone (untreated) or IgG (1.6 μg/mL) as controls. PC3 cells were harvested, pelleted, and resuspended in adhesion buffer; 5×10^4 cells were plated on each pre-loaded well and allowed to settle at 37 °C. After 1 h, the medium was gently removed and wells were washed 3–5 times with adhesion buffer to remove non-adhered cells. Adhered PC3 cells were then stained with 0.1 % crystal violet solution for 1 h at room temperature. The excess crystal violet was gently washed with tap water, and the wells were air-dried. After dye elution with 100 μL of methanol, the O.D. of stained PC3 cells was measured at 600 nm in a spectrophotometer (Thermo-Scientific Multiskan Spectrum) using ScanIt software 2.4.4.

Adhesion assays

DU145 adhesion assays—Cell adhesion assays were performed as previously described [76]. Wells were pre-coated with collagen (354,236, Corning) 50 μg/ml, laminin (L6274, Sigma) 10 μg/ml, human plasma-derived vitronectin 5 μg/ml, human plasma-derived fibrinogen 50, 15 or 5 μg/ml, or 1 % heat denatured BSA as control. For another set of experiments, prior to the addition of cells, wells were pre-loaded with 100 μL of LM609 (10 or 20 μg/mL) diluted in adhesion buffer (SFM, 0.5 % BSA); IgG1 (10 or 20 μg/mL in adhesion buffer) or adhesion buffer alone (untreated) were used as controls. The O.D. of stained DU145 cells was measured at 600 nm in a spectrophotometer (Thermo-Scientific Multiskan Spectrum) using ScanIt software 2.4.4.

Monocyte adhesion assays—PBMCs were incubated with either PBS, healthy donor-derived sEVs, or PrCa patient-derived sEVs for 48 h prior to the assay. In another set of experiments, PBMCs were incubated with sEVs derived from PC3 cells transfected with two shRNA constructs that target RTN4RL2 or with a non-targeting scrambled control shRNA. Non-treated 96 well plates were coated with 150 μL of fibronectin 10 μg/mL or 1 % heat denatured filtered BSA as control overnight at 4 °C. On the day of the assay, the coated wells were blocked with 150 μL of 1 % BSA in PBS for 30 min at room temperature followed by two washes with SFM. Non-adherent PBMCs were discarded and monocytes attached to wells were washed with PBS and gently scraped from the 6-well plates. Cells were pelleted and resuspended in SFM; afterwards, they were plated ($2.5–3 \times 10^5$/150 μL per well, 2–3 replicates per condition) and allowed to settle at 37 °C for 4 h. After 4 h, medium was gently removed and the wells were washed 3 times with SFM to remove the non-adhered cells. Adhered cells were fixed with paraformaldehyde (3 % in PBS) for 30 min at room temperature, followed by two washes with PBS; 0.1 % crystal violet solution was used for staining. The excess crystal violet was gently washed with tap water, and the wells were air-dried. The attached cells were imaged (3 different FOV/well, FOV = 0.044 mm diameter) using an inverted microscope (Nikon Eclipse TS100) that generated a 164×123 mm image. The number of cells for each field was counted manually, and the mean number ± SEM for each condition was reported.

Flow cytometry analysis—Flow cytometric phenotyping of human PBMCs from healthy donors was performed as follows: PBMCs (1×10^6 cells/tube) were aliquoted into flow tubes (Falcon, 352,008) and stained with combinations of mouse conjugated Abs to human for 25 min at 4 °C. Samples were washed with PBS and analyzed immediately by flow cytometry. Flow data were acquired using a Celesta cytometer with Diva 8.0 (BD Biosciences), and post-collection analysis was performed with FlowJo software (FlowJo, LLC).

Statistical analysis

For the PDX experiments, tumor volumes were compared for all groups using the Wilcoxon rank-sum test. For tumor growth, a linear mixed effects model was used to model log 10 transformed tumor volumes. Fixed effects were day, group, and day by group interaction to allow for estimation of the average slope by group. A random intercept and slope term were included to account for animal-specific deviations from the group averages. Slope estimates were back-transformed (10êstimate) to obtain the geometric mean ratio (GMR) representing the multiplicative change in tumor volume per day. If the test of any group differences for GMR was significant, pairwise comparisons were performed with p-values adjusted using the Bonferroni method. Analysis of tumor volumes was performed using SAS version 9.4, SAS Institute, Cary, NC.

For the flow cytometry analysis, paired two group comparisons were analyzed using paired *t*-test; multiple group comparisons with matched samples were analyzed using ANOVA for repeated measures with Tukey's multiple comparisons test. SAS 9.4 and Prism 7 were used for data analysis.

For adhesion assays, ANOVA and paired *t*-tests were performed using GraphPad Prism 9 version 9.4.1(458) for macOS, GraphPad Software, San Diego, California USA, www.graphpad.com.

Supplementary Material

Refer to Web version on PubMed Central for supplementary material.

Acknowledgements

The authors would like to thank S. Yadav and U. Naik for providing discarded, de-identified healthy donors' plasma and S. Cremin and S. Herder for discarded, de-identified prostate cancer patients' plasma (Thomas Jefferson Biobank repository). We would also like to thank Dr Mark Ginsberg, UCSD, for his generous gift of LIBS1 and 6 antibodies and Dr Yoshi Takada, UC Davis, for providing information on the use of LIBS antibodies. We thank H. Wetterstein for helpful discussion. We would like to thank the animal facility of the Sidney Kimmel Cancer Center (SKCC) for assistance with mice care. We thank Dr Lei Yu of the SKCC Flow Cytometry and Human Immune Monitoring Core and Dr Zhijiu Zhong of the Translational Research/Pathology Shared Resource at Thomas Jefferson University for technical support.

Funding

This study was supported by R01 CA224769, DoD W81XWH2210826, Philadelphia Prostate Cancer Biome Project (LRL), Cure Funds of the PA Dept of Health (LRL and DCH), the Prostate Cancer Foundation Young Investigator award (FQ and AT), and P01 HL154811 (EFP). The research reported in this publication utilized the Thomas Jefferson Biobank repository, the Flow Cytometry and Human Immune Monitoring Core and the Translational Research/Pathology Shared Resource at the Sidney Kimmel Cancer Center (Thomas Jefferson

University, Philadelphia, PA) that the NCI supports under award number P30CA056036. Dr. Testa is a Visiting Scholar at Thomas Jefferson University partially funded by University of Turin, Italy.

Data availability

No data were used for the research described in the article.

Abbreviations:

ADPrCa	adenocarcinoma of the prostate
FOV	field of view
IDG	iodixanol density gradient
MFI	mean fluorescent intensity
NED	neuroendocrine differentiation
NEPrCa	neuroendocrine prostate cancer
NTA	nanoparticle tracking analysis
PDX	patient-derived xenograft
PrCa	prostate cancer
PSA	prostate-specific antigen
SCID	severe combined immunodeficient
sEVs	small extracellular vesicles
TAM	tumor-associated macrophages
TMA	tissue microarrays
TME	tumor microenvironment

References

[1]. Hamidi H, Ivaska J, Every step of the way: integrins in cancer progression and metastasis, Nat. Rev. Cancer 18 (9) (2018) 533–548. [PubMed: 30002479]

[2]. Zheng DQ, Woodard AS, Fornaro M, Tallini G, Languino LR, Prostatic carcinoma cell migration via αVβ3 integrin is modulated by a focal adhesion kinase pathway, Cancer Res. 59 (7) (1999) 1655–1664. [PubMed: 10197643]

[3]. Desgrosellier JS, Cheresh DA, Integrins in cancer: biological implications and therapeutic opportunities, Nat. Rev. Cancer 10 (1) (2010) 9–22. [PubMed: 20029421]

[4]. Weber MR, Zuka M, Lorger M, Tschan M, Torbett BE, Zijlstra A, Quigley JP, Staflin K, Eliceiri BP, Krueger JS, Marchese P, Ruggeri ZM, Felding BH, Activated tumor cell integrin alphavbeta3 cooperates with platelets to promote extravasation and metastasis from the blood stream, Thromb. Res. 140 (Suppl 1) (2016) S27–S36. [PubMed: 27067975]

[5]. Jin H, Varner J, Integrins: roles in cancer development and as treatment targets, Br. J. Cancer 90 (3) (2004) 561–565. [PubMed: 14760364]

[6]. Mulgrew K, Kinneer K, Yao XT, Ward BK, Damschroder MM, Walsh B, Mao SY, Gao C, Kiener PA, Coats S, Kinch MS, Tice DA, Direct targeting of alphavbeta3 integrin on tumor cells with a monoclonal antibody, Abegrin, Mol. Cancer Ther. 5 (12) (2006) 3122–3129. [PubMed: 17172415]

[7]. Quaglia F, Krishn SR, Daaboul GG, Sarker S, Pippa R, Domingo-Domenech J, Kumar G, Fortina P, McCue P, Kelly WK, Beltran H, Liu Q, Languino LR, Small extracellular vesicles modulated by αVβ3 integrin induce neuroendocrine differentiation in recipient cancer cells, J. Extracell. Vesicles 9 (1) (2020), 1761072. [PubMed: 32922691]

[8]. Quaglia F, Krishn SR, Wang Y, Goodrich DW, McCue P, Kossenkov AV, Mandigo AC, Knudsen KE, Weinreb PH, Corey E, Kelly WK, Languino LR, Differential expression of αVβ3 and αVβ6 integrins in prostate cancer progression, PLoS ONE 16 (1) (2021), e0244985. [PubMed: 33481853]

[9]. Beltran H, Tomlins S, Aparicio A, Arora V, Rickman D, Ayala G, Huang J, True L, Gleave ME, Soule H, Logothetis C, Rubin MA, Aggressive variants of castration resistant prostate cancer, Clin. Cancer Res. 20 (11) (2014) 2846–2850. [PubMed: 24727321]

[10]. Palmgren JS, Karavadia SS, Wakefield MR, Unusual and underappreciated: small cell carcinoma of the prostate, Semin. Oncol. 34 (1) (2007) 22–29. [PubMed: 17270662]

[11]. Beltran H, Hruszkewycz A, Scher HI, Hildesheim J, Isaacs J, Yu EY, Kelly K, Lin D, Dicker A, Arnold J, Hecht T, Wicha M, Sears R, Rowley D, White R, Gulley JL, Lee J, Diaz Meco M, Small EJ, Shen M, Knudsen K, Goodrich DW, Lotan T, Zoubeidi A, Sawyers CL, Rudin CM, Loda M, Thompson T, Rubin MA, Tawab-Amiri A, Dahut W, Nelson PS, The role of lineage plasticity in prostate cancer therapy resistance, Clin. Cancer Res. 25 (23) (2019) 6916–6924. [PubMed: 31363002]

[12]. Abida W, Cyrta J, Heller G, Prandi D, Armenia J, Coleman I, Cieslik M, Benelli M, Robinson D, Van Allen EM, Sboner A, Fedrizzi T, Mosquera JM, Robinson BD, De Sarkar N, Kunju LP, Tomlins S, Wu YM, Nava Rodrigues D, Loda M, Gopalan A, Reuter VE, Pritchard CC, Mateo J, Bianchini D, Miranda S, Carreira S, Rescigno P, Filipenko J, Vinson J, Montgomery RB, Beltran H, Heath EI, Scher HI, Kantoff PW, Taplin ME, Schultz N, deBono JS, Demichelis F, Nelson PS, Rubin MA, Chinnaiyan AM, Sawyers CL, Genomic correlates of clinical outcome in advanced prostate cancer, Proc. Natl. Acad. Sci. USA 116 (23) (2019) 11428–11436. [PubMed: 31061129]

[13]. Beltran H, Prandi D, Mosquera JM, Benelli M, Puca L, Cyrta J, Marotz C, Giannopoulou E, Chakravarthi BV, Varambally S, Tomlins SA, Nanus DM, Tagawa ST, Van Allen EM, Elemento O, Sboner A, Garraway LA, Rubin MA, Demichelis F, Divergent clonal evolution of castration-resistant neuroendocrine prostate cancer, Nat. Med. 22 (3) (2016) 298–305. [PubMed: 26855148]

[14]. Kwon OJ, Zhang L, Jia D, Zhou Z, Li Z, Haffner M, Lee JK, True L, Morrissey C, Xin L, De novo induction of lineage plasticity from human prostate luminal epithelial cells by activated AKT1 and c-Myc, Oncogene 39 (48) (2020) 7142–7151. [PubMed: 33009488]

[15]. Aggarwal R, Huang J, Alumkal JJ, Zhang L, Feng FY, Thomas GV, Weinstein AS, Friedl V, Zhang C, Witte ON, Lloyd P, Gleave M, Evans CP, Youngren J, Beer TM, Rettig M, Wong CK, True L, Foye A, Playdle D, Ryan CJ, Lara P, Chi KN, Uzunangelov V, Sokolov A, Newton Y, Beltran H, Demichelis F, Rubin MA, Stuart JM, Small EJ, Clinical and genomic characterization of treatment-emergent small-cell neuroendocrine prostate cancer: a multi-institutional prospective study, J. Clin. Oncol. 36 (24) (2018) 2492–2503. [PubMed: 29985747]

[16]. Bluemn EG, Coleman IM, Lucas JM, Coleman RT, Hernandez-Lopez S, Tharakan R, Bianchi-Frias D, Dumpit RF, Kaipainen A, Corella AN, Yang YC, Nyquist MD, Mostaghel E, Hsieh AC, Zhang X, Corey E, Brown LG, Nguyen HM, Pienta K, Ittmann M, Schweizer M, True LD, Wise D, Rennie PS, Vessella RL, Morrissey C, Nelson PS, Androgen receptor pathway-independent prostate cancer is sustained through FGF signaling, Cancer Cell 32 (4) (2017) 474–489. [PubMed: 29017058]

[17]. Hoshino A, Costa-Silva B, Shen TL, Rodrigues G, Hashimoto A, Tesic Mark M, Molina H, Kohsaka S, Di Giannatale A, Ceder S, Singh S, Williams C, Soplop N, Uryu K, Pharmer L, King T, Bojmar L, Davies AE, Ararso Y, Zhang T, Zhang H, Hernandez J, Weiss JM, Dumont-Cole VD, Kramer K, Wexler LH, Narendran A, Schwartz GK, Healey JH, Sandstrom P, Labori KJ, Kure EH, Grandgenett PM, Hollingsworth MA, de Sousa M, Kaur S, Jain M, Mallya K, Batra SK, Jarnagin WR, Brady MS, Muller V, Pantel K, Minn AJ, Bissell MJ, Garcia BA, Kang

Y, Rajasekhar VK, Ghajar CM, Matei I, Peinado H, Bromberg J, Lyden D, Tumour exosome integrins determine organotropic metastasis, Nature 527 (7578) (2015) 329–335. [PubMed: 26524530]

[18]. Wortzel I, Dror S, Kenific CM, Lyden D, Exosome-mediated metastasis: communication from a distance, Dev. Cell 49 (3) (2019) 347–360. [PubMed: 31063754]

[19]. Zhang H, Freitas D, Kim HS, Fabijanic K, Li Z, Chen H, Mark MT, Molina H, Martin AB, Bojmar L, Fang J, Rampersaud S, Hoshino A, Matei I, Kenific CM, Nakajima M, Mutvei AP, Sansone P, Buehring W, Wang H, Jimenez JP, Cohen-Gould L, Paknejad N, Brendel M, Manova-Todorova K, Magalhaes A, Ferreira JA, Osorio H, Silva AM, Massey A, Cubillos-Ruiz JR, Galletti G, Giannakakou P, Cuervo AM, Blenis J, Schwartz R, Brady MS, Peinado H, Bromberg J, Matsui H, Reis CA, Lyden D, Identification of distinct nanoparticles and subsets of extracellular vesicles by asymmetric flow field-flow fractionation, Nat. Cell. Biol 20 (3) (2018) 332–343. [PubMed: 29459780]

[20]. Peinado H, Lavotshkin S, Lyden D, The secreted factors responsible for pre-metastatic niche formation: old sayings and new thoughts, Semin. Cancer Biol. 21 (2) (2011) 139–146. [PubMed: 21251983]

[21]. Fedele C, Singh A, Zerlanko BJ, Iozzo RV, Languino LR, The αVβ6 integrin is transferred intercellularly via exosomes, J. Biol. Chem. 290 (8) (2015) 4545–4551. [PubMed: 25568317]

[22]. DeRita RM, Sayeed A, Garcia V, Krishn SR, Shields CD, Sarker S, Friedman A, McCue P, Molugu SK, Rodeck U, Dicker AP, Languino LR, Tumor-derived extracellular vesicles require beta1 integrins to promote anchorage-independent growth, iScience 14 (2019) 199–209. [PubMed: 30981115]

[23]. Singh A, Fedele C, Lu H, Nevalainen MT, Keen JH, Languino LR, Exosome-mediated transfer of alphavbeta3 integrin from tumorigenic to nontumorigenic cells promotes a migratory phenotype, Mol. Cancer Res. 14 (11) (2016) 1136–1146. [PubMed: 27439335]

[24]. Krishn SR, Salem I, Quaglia F, Naranjo NM, Agarwal E, Liu Q, Sarker S, Kopenhaver J, McCue PA, Weinreb PH, Violette SM, Altieri DC, Languino LR, The αVβ6 integrin in cancer cell-derived small extracellular vesicles enhances angiogenesis, J. Extracell. Vesicles 9 (1) (2020), 1763594. [PubMed: 32595914]

[25]. Zheng B, Atwal J, Ho C, Case L, He XL, Garcia KC, Steward O, Tessier-Lavigne M, Genetic deletion of the Nogo receptor does not reduce neurite inhibition *in vitro* or promote corticospinal tract regeneration *in vivo*, Proc. Natl. Acad. Sci. USA 102 (4) (2005) 1205–1210. [PubMed: 15647357]

[26]. Thery C, Witwer KW, Aikawa E, Alcaraz MJ, Anderson JD, Andriantsitohaina R, Antoniou A, Arab T, Archer F, Atkin-Smith GK, Ayre DC, Bach JM, Minimal information for studies of extracellular vesicles 2018 (MISEV2018): a position statement of the International Society for Extracellular Vesicles and update of the MISEV2014 guidelines, J. Extracell. Vesicles 7 (1) (2018), 1535750. [PubMed: 30637094]

[27]. Chevillet JR, Kang Q, Ruf IK, Briggs HA, Vojtech LN, Hughes SM, Cheng HH, Arroyo JD, Meredith EK, Gallichotte EN, Pogosova-Agadjanyan EL, Morrissey C, Stirewalt DL, Hladik F, Yu EY, Higano CS, Tewari M, Quantitative and stoichiometric analysis of the microRNA content of exosomes, Proc. Natl. Acad. Sci. USA 111 (41) (2014) 14888–14893. [PubMed: 25267620]

[28]. Jafari N, Llevenes P, Denis GV, Exosomes as novel biomarkers in metabolic disease and obesity-related cancers, Nat. Rev. Endocrinol. 18 (6) (2022) 327–328. [PubMed: 35361917]

[29]. Cook LM, Shay G, Araujo A, Lynch CC, Integrating new discoveries into the “vicious cycle” paradigm of prostate to bone metastases, Cancer Metastasis Rev. 33 (2–3) (2014) 511–525. [PubMed: 24414228]

[30]. Brena D, Huang MB, Bond V, Extracellular vesicle-mediated transport: reprogramming a tumor microenvironment conducive with breast cancer progression and metastasis, Transl. Oncol. 15 (1) (2022), 101286. [PubMed: 34839106]

[31]. Datta A, Kim H, McGee L, Johnson AE, Talwar S, Marugan J, Southall N, Hu X, Lal M, Mondal D, Ferrer M, Abdel-Mageed AB, High-throughput screening identified selective inhibitors of exosome biogenesis and secretion: a drug repurposing strategy for advanced cancer, Sci. Rep. 8 (1) (2018) 8161. [PubMed: 29802284]

[32]. Pignot V, Hein AE, Barske C, Wiessner C, Walmsley AR, Kaupmann K, Mayeur H, Sommer B, Mir AK, Frentzel S, Characterization of two novel proteins, NgRH1 and NgRH2, structurally and biochemically homologous to the Nogo-66 receptor, J. Neurochem. 85 (3) (2003) 717–728. [PubMed: 12694398]

[33]. Semavina M, Saha N, Kolev MV, Goldgur Y, Giger RJ, Himanen JP, Nikolov DB, Crystal structure of the Nogo-receptor-2, Protein Sci. 20 (4) (2011) 684–689. [PubMed: 21308849]

[34]. Quaglia F, Krishn SR, Sossey-Alaoui K, Rana PS, Pluskota E, Park PH, Shields CD, Lin S, McCue P, Kossenkov AV, Wang Y, Goodrich DW, Ku SY, Beltran H, Kelly WK, Corey E, Klose M, Bandtlow C, Liu Q, Altieri DC, Plow EF, Languino LR, The NOGO receptor NgR2, a novel αVβ3 integrin effector, induces neuroendocrine differentiation in prostate cancer, Sci. Rep. 12 (1) (2022) 18879. [PubMed: 36344556]

[35]. Venkatesh K, Chivatakarn O, Lee H, Joshi PS, Kantor DB, Newman BA, Mage R, Rader C, Giger RJ, The Nogo-66 receptor homolog NgR2 Is a sialic acid-dependent receptor selective for myelin-associated glycoprotein, J. Neurosci. 25 (4) (2005) 808–822. [PubMed: 15673660]

[36]. Robak LA, Venkatesh K, Lee H, Raiker SJ, Duan Y, Lee-Osbourne J, Hofer T, Mage RG, Rader C, Giger RJ, Molecular basis of the interactions of the Nogo-66 receptor and its homolog NgR2 with myelin-associated glycoprotein: development of NgROMNI-Fc, a novel antagonist of CNS myelin inhibition, J. Neurosci. 29 (18) (2009) 5768–5783. [PubMed: 19420245]

[37]. Wang KC, Kim JA, Sivasankaran R, Segal R, He Z, P75 interacts with the Nogo receptor as a co-receptor for Nogo, MAG and OMgp, Nature 420 (6911) (2002) 74–78. [PubMed: 12422217]

[38]. Mi S, Lee X, Shao Z, Thill G, Ji B, Relton J, Levesque M, Allaire N, Perrin S, Sands B, Crowell T, Cate RL, McCoy JM, Pepinsky RB, LINGO-1 is a component of the Nogo-66 receptor/p75 signaling complex, Nat. Neurosci. 7 (3) (2004) 221–228. [PubMed: 14966521]

[39]. David S, Fry EJ, Lopez-Vales R, Novel roles for Nogo receptor in inflammation and disease, Trends Neurosci. 31 (5) (2008) 221–226. [PubMed: 18394723]

[40]. Dubreuil CI, Winton MJ, McKerracher L, Rho activation patterns after spinal cord injury and the role of activated Rho in apoptosis in the central nervous system, J. Cell. Biol. 162 (2) (2003) 233–243. [PubMed: 12860969]

[41]. Xiao Y, Yu D, Tumor microenvironment as a therapeutic target in cancer, Pharmacol. Ther. 221 (2021), 107753. [PubMed: 33259885]

[42]. Han C, Deng Y, Xu W, Liu Z, Wang T, Wang S, Liu J, Liu X, The roles of tumor-associated macrophages in prostate cancer, J. Oncol. 2022 (2022), 8580043. [PubMed: 36117852]

[43]. Sica A, Schioppa T, Mantovani A, Allavena P, Tumour-associated macrophages are a distinct M2 polarised population promoting tumour progression: potential targets of anti-cancer therapy, Eur. J. Cancer 42 (6) (2006) 717–727. [PubMed: 16520032]

[44]. Larionova I, Tuguzbaeva G, Ponomaryova A, Stakheyeva M, Cherdyntseva N, Pavlov V, Choinzonov E, Kzhyshkowska J, Tumor-associated macrophages in human breast, colorectal, lung, ovarian and prostate cancers, Front. Oncol. 10 (2020), 566511. [PubMed: 33194645]

[45]. Jiang C, Jiang Z, Sha G, Wang D, Tang D, Small extracellular vesicle-mediated metabolic reprogramming: from tumors to pre-metastatic niche formation, Cell Commun. Signal. 21 (1) (2023) 116. [PubMed: 37208722]

[46]. Tian JW, Zhang HJ, Li SY, Guo YL, Chen G, Yu ZL, Tumor cell-derived extracellular vesicles in modulating phenotypes and immune functions of macrophages: mechanisms and therapeutic applications, J. Cancer 14 (8) (2023) 1321–1334. [PubMed: 37283792]

[47]. Lundholm M, Hagglof C, Wikberg ML, Stattin P, Egevad L, Bergh A, Wikstrom P, Palmqvist R, Edin S, Secreted factors from colorectal and prostate cancer cells skew the immune response in opposite directions, Sci. Rep. 5 (2015) 15651. [PubMed: 26503803]

[48]. Boutilier AJ, Elsawa SF, Macrophage polarization states in the tumor microenvironment, Int. J. Mol. Sci. 22 (13) (2021), 10.3390/ijms22136995.

[49]. Baig MS, Roy A, Rajpoot S, Liu D, Savai R, Banerjee S, Kawada M, Faisal SM, Saluja R, Saqib U, Ohishi T, Wary KK, Tumor-derived exosomes in the regulation of macrophage polarization, Inflamm. Res. 69 (5) (2020) 435–451. [PubMed: 32162012]

[50]. Mezzasoma L, Costanzi E, Scarpelli P, Talesa VN, Bellezza I, Extracellular vesicles from human advanced-stage prostate cancer cells modify the inflammatory response of microenvironment-residing cells, Cancers 11 (9) (2019), 10.3390/cancers11091276 (Basel).

[51]. Peng Y, Zhao M, Hu Y, Guo H, Zhang Y, Huang Y, Zhao L, Chai Y, Wang Z, Blockade of exosome generation by GW4869 inhibits the education of M2 macrophages in prostate cancer, BMC Immunol. 23 (1) (2022) 37. [PubMed: 35941539]

[52]. Lu H, Bowler N, Harshyne LA, Hooper DC, Krishn SR, Kurtoglu S, Fedele C, Liu Q, Tang HY, Kossenkov AV, Kelly WK, Wang K, Kean RB, Weinreb PH, Yu L, Dutta A, Fortina P, Ertel A, Stanczak M, Forsberg F, Gabrilovich DI, Speicher DW, Altieri DC, Languino LR, Exosomal αvβ6 integrin is required for monocyte M2 polarization in prostate cancer, Matrix Biol. 70 (2018) 20–35. [PubMed: 29530483]

[53]. Brooks PC, Stromblad S, Klemke R, Visscher D, Sarkar FH, Cheresh DA, Antiintegrin alpha v beta 3 blocks human breast cancer growth and angiogenesis in human skin, J. Clin. Investig. 96 (4) (1995) 1815–1822. [PubMed: 7560073]

[54]. Wettersten HI, Weis SM, Pathria P, Von Schalscha T, Minami T, Varner JA, Cheresh DA, Arming tumor-associated macrophages to reverse epithelial cancer progression, Cancer Res. 79 (19) (2019) 5048–5059. [PubMed: 31416839]

[55]. Borst AJ, James ZM, Zagotta WN, Ginsberg M, Rey FA, DiMaio F, Backovic M, Veesler D, The therapeutic antibody lm609 selectively inhibits ligand binding to human alphaVbeta3 integrin via steric hindrance, Structure 25 (11) (2017) 1732–1739, e5. [PubMed: 29033288]

[56]. Cheresh DA, Human endothelial cells synthesize and express an Arg-Gly-Asp-directed adhesion receptor involved in attachment to fibrinogen and von Willebrand factor, Proc. Natl. Acad. Sci. USA 84 (18) (1987) 6471–6475. [PubMed: 2442758]

[57]. Nguyen HM, Vessella RL, Morrissey C, Brown LG, Coleman IM, Higano CS, Mostaghel EA, Zhang X, True LD, Lam HM, Roudier M, Lange PH, Nelson PS, Corey E, LuCaP prostate cancer patient-derived xenografts reflect the molecular heterogeneity of advanced disease and serve as models for evaluating cancer therapeutics, Prostate 77(6) (2017) 654–671. [PubMed: 28156002]

[58]. Krishn SR, Singh A, Bowler N, Duffy AN, Friedman A, Fedele C, Kurtoglu S, Tripathi SK, Wang K, Hawkins A, Sayeed A, Goswami CP, Thakur ML, Iozzo RV, Peiper SC, Kelly WK, Languino LR, Prostate cancer sheds the αvβ3 integrin *in vivo* through exosomes, Matrix Biol. 77 (2019) 41–57. [PubMed: 30098419]

[59]. Nielsen MC, Andersen MN, Moller HJ, Monocyte isolation techniques significantly impact the phenotype of both isolated monocytes and derived macrophages *in vitro*, Immunology 159 (1) (2020) 63–74. [PubMed: 31573680]

[60]. Charo IF, Nannizzi L, Smith JW, Cheresh DA, The vitronectin receptor αVβ3 binds fibronectin and acts in concert with α5β1 in promoting cellular attachment and spreading on fibronectin, J. Cell. Biol. 111 (1990) 2795–2800, 6 Pt 1. [PubMed: 1703545]

[61]. Cheresh DA, Spiro RC, Biosynthetic and functional properties of an Arg-Gly-Asp-directed receptor involved in human melanoma cell attachment to vitronectin, fibrinogen, and von Willebrand factor, J. Biol. Chem. 262 (36) (1987) 17703–17711. [PubMed: 2447074]

[62]. Sugahara KN, Teesalu T, Karmali PP, Kotamraju VR, Agemy L, Girard OM, Hanahan D, Mattrey RF, Ruoslahti E, Tissue-penetrating delivery of compounds and nanoparticles into tumors, Cancer Cell 16 (6) (2009) 510–520. [PubMed: 19962669]

[63]. Suzuki K, Kunisada Y, Miyamura N, Eikawa S, Hurtado de Mendoza T, Mose ES, Lu C, Kuroda Y, Ruoslahti E, Lowy AM, Sugahara KN, Tumor-resident regulatory T cells in pancreatic cancer express the αVβ5 integrin as a targetable activation marker, bioRxiv (2023).

[64]. Takagi J, Petre BM, Walz T, Springer TA, Global conformational rearrangements in integrin extracellular domains in outside-in and inside-out signaling, Cell 110 (5) (2002) 599–611. [PubMed: 12230977]

[65]. Xiong JP, Stehle T, Zhang R, Joachimiak A, Frech M, Goodman SL, Arnaout MA, Crystal structure of the extracellular segment of integrin αVβ3 in complex with an Arg-Gly-Asp ligand, Science 296 (5565) (2002) 151–155. [PubMed: 11884718]

[66]. Xiao T, Takagi J, Coller BS, Wang JH, Springer TA, Structural basis for allostery in integrins and binding to fibrinogen-mimetic therapeutics, Nature 432 (7013) (2004) 59–67. [PubMed: 15378069]

[67]. Yokoyama K, Erickson HP, Ikeda Y, Takada Y, Identification of amino acid sequences in fibrinogen γ-chain and tenascin C C-terminal domains critical for binding to integrin αVβ3, J. Biol. Chem. 275 (22) (2000) 16891–16898. [PubMed: 10747940]

[68]. Pruitt HC, Guan Y, Liu H, Carey AE, Brennen WN, Lu J, Joshu C, Weeraratna A, Lotan TL, Karin Eisinger-Mathason TS, Gerecht S, Collagen VI deposition mediates stromal T cell trapping through inhibition of T cell motility in the prostate tumor microenvironment, Matrix Biol. 121 (2023) 90–104. [PubMed: 37331435]

[69]. Yamada Y, Beltran H, Clinical and biological features of neuroendocrine prostate cancer, Curr. Oncol. Rep. 23 (2) (2021) 15. [PubMed: 33433737]

[70]. Tkach M, Thalmensi J, Timperi E, Gueguen P, Nevo N, Grisard E, Sirven P, Cocozza F, Gouronnec A, Martin-Jaular L, Jouve M, Delisle F, Manel N, Rookhuizen DC, Guerin CL, Soumelis V, Romano E, Segura E, Thery C, Extracellular vesicles from triple negative breast cancer promote pro-inflammatory macrophages associated with better clinical outcome, Proc. Natl. Acad. Sci. USA 119 (17) (2022), 10.1073/pnas.2107394119.

[71]. Adamczyk AM, Leicaj ML, Fabiano MP, Cabrerizo G, Bannoud N, Croci DO, Witwer KW, Remes Lenicov F, Ostrowski M, Perez PS, Extracellular vesicles from human plasma dampen inflammation and promote tissue repair functions in macrophages, J. Extracell. Vesicles 12 (6) (2023) e12331. [PubMed: 37272889]

[72]. Frelinger AL III, Cohen I, Plow EF, Smith MA, Roberts J, Lam SC, Ginsberg MH, Selective inhibition of integrin function by antibodies specific for ligand-occupied receptor conformers, J. Biol. Chem. 265 (11) (1990) 6346–6352. [PubMed: 2318856]

[73]. Pelletier AJ, Kunicki T, Quaranta V, Activation of the integrin αVβ3 involves a discrete cation-binding site that regulates conformation, J. Biol. Chem. 271 (3) (1996) 1364–1370. [PubMed: 8576125]

[74]. Goel HL, Sayeed A, Breen M, Zarif MJ, Garlick DS, Leav I, Davis RJ, Fitzgerald TJ, Morrione A, Hsieh CC, Liu Q, Dicker AP, Altieri DC, Languino LR, β1 integrins mediate resistance to ionizing radiation *in vivo* by inhibiting c-Jun amino terminal kinase 1, J. Cell. Physiol. 228 (7) (2013) 1601–1609. [PubMed: 23359252]

[75]. Salem I, Naranjo NM, Singh A, DeRita R, Krishn SR, Sirman LS, Quaglia F, Duffy A, Bowler N, Sayeed A, Languino LR, Methods for extracellular vesicle isolation from cancer cells, Cancer Drug Resist. 3 (3) (2020) 371–384. [PubMed: 33062957]

[76]. Krishn SR, Garcia V, Naranjo NM, Quaglia F, Shields CD, Harris MA, Kossenkov AV, Liu Q, Corey E, Altieri DC, Languino LR, Small extracellular vesicle-mediated ITGB6 siRNA delivery downregulates the alphaVbeta6 integrin and inhibits adhesion and migration of recipient prostate cancer cells, Cancer Biol. Ther. 23 (1) (2022) 173–185. [PubMed: 35188070]

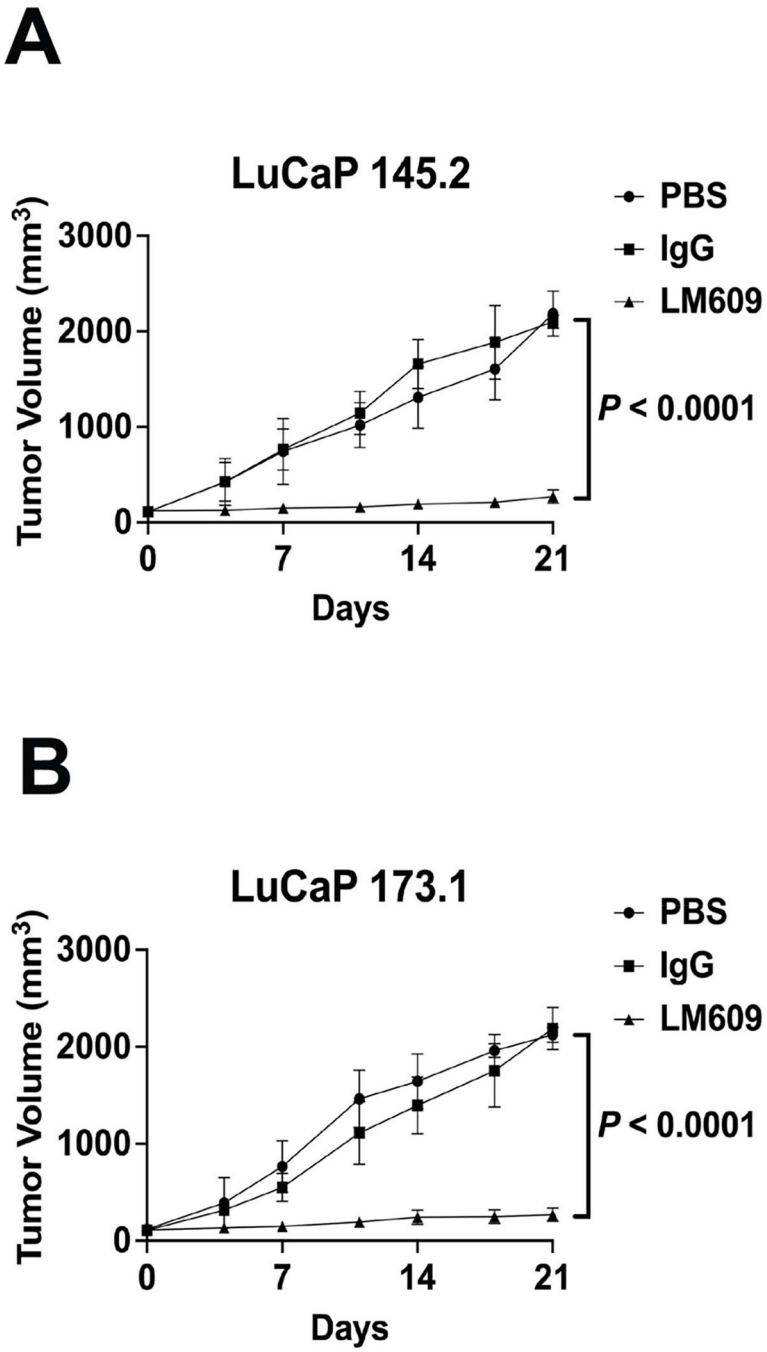

Fig. 1.

αVβ3 integrin inhibition by the LM609 antibody reduces NEPrCa LuCaP tumor growth. LuCaP 145.2 and LuCaP 173.1 bits were implanted subcutaneously into CB-17 SCID mice. Mice carrying tumors of ~100–150 mm3 were treated intraperitoneally twice weekly for 3 weeks, with LM609 (LuCaP 145.2, $n = 5$; LuCaP 173.1, $n = 5$); IgG1 (LuCaP 145.2, $n = 5$; LuCaP 173.1, $n = 5$) or PBS (LuCaP 145.2, $n = 5$; LuCaP 173.1, $n = 5$). (**A**) LuCaP 145.2 and (**B**) LuCaP 173.1 xenograft volumes were measured twice weekly during treatment.

P-values are indicated in the figure. Significance was calculated using the Mann-Whitney test.

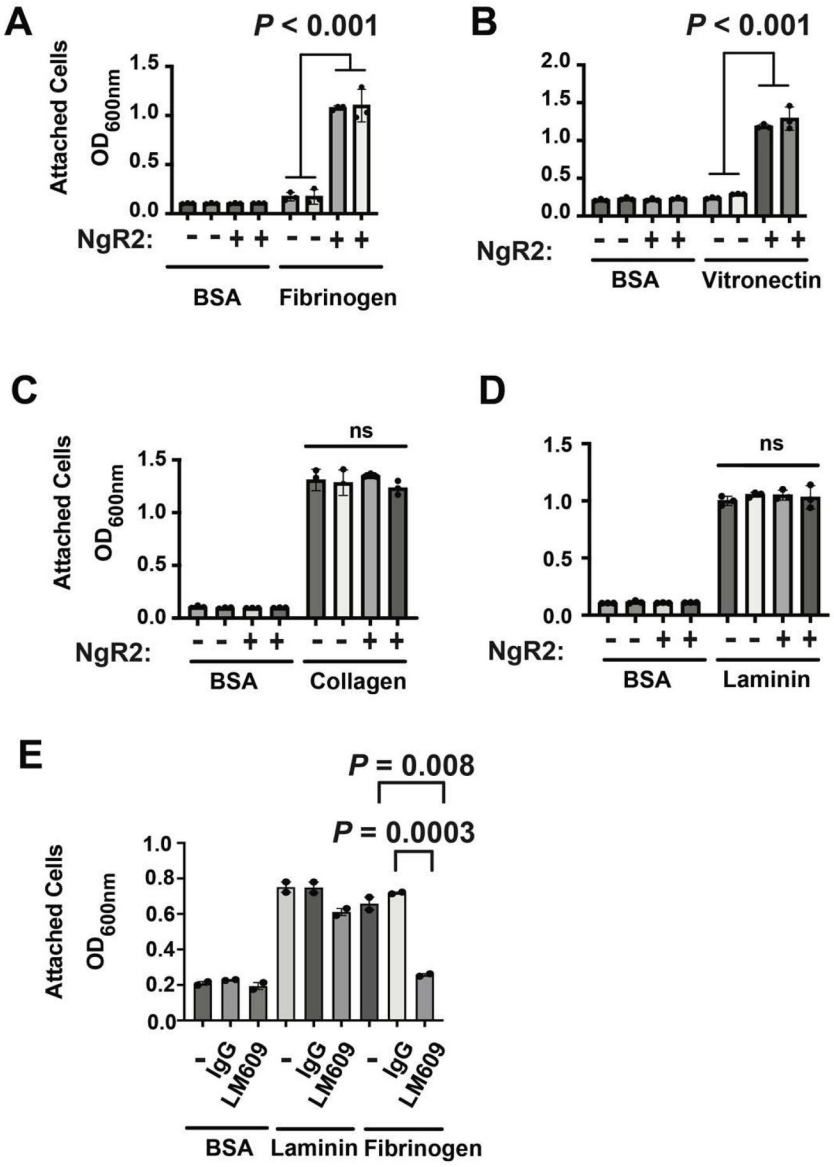

Fig. 2.

NgR2 expression increases cell adhesion to αVβ3 ligands. (**A**-**D**) DU145 NgR2 cells (+) or DU145 Mock cells not expressing NgR2 (−) were seeded (5×10^4 cells/well, 3 replicates) for 1 h on ECM proteins (fibrinogen, vitronectin, collagen, or laminin) or BSA (1 %) coated wells. (A) Fibrinogen (50 μg/mL) adhesion. (B) Vitronectin (5 μg/mL) adhesion. (C) Collagen (50 μg/mL) adhesion. (D) Laminin (10 μg/mL) adhesion. (**E**) DU145 NgR2 cells were seeded (5×10^4 cells/well, 2 replicates) for 1 h on ECM proteins (fibrinogen 15 μg/mL or laminin 10 μg/mL) or BSA (1 %) coated wells. Wells were pre-incubated with LM609 (20 μg/mL); treatment with IgG1 (20 μg/mL) or adhesion buffer alone (−) were used as controls. (**A**-**E**) Bar graphs represent the degree of cell adhesion quantified as optical density (O.D.) of crystal violet staining measured at 600 nm. The values are presented as mean ± standard error of the mean (SEM); P values were calculated using *t*-test ($n = 3$ for each condition).

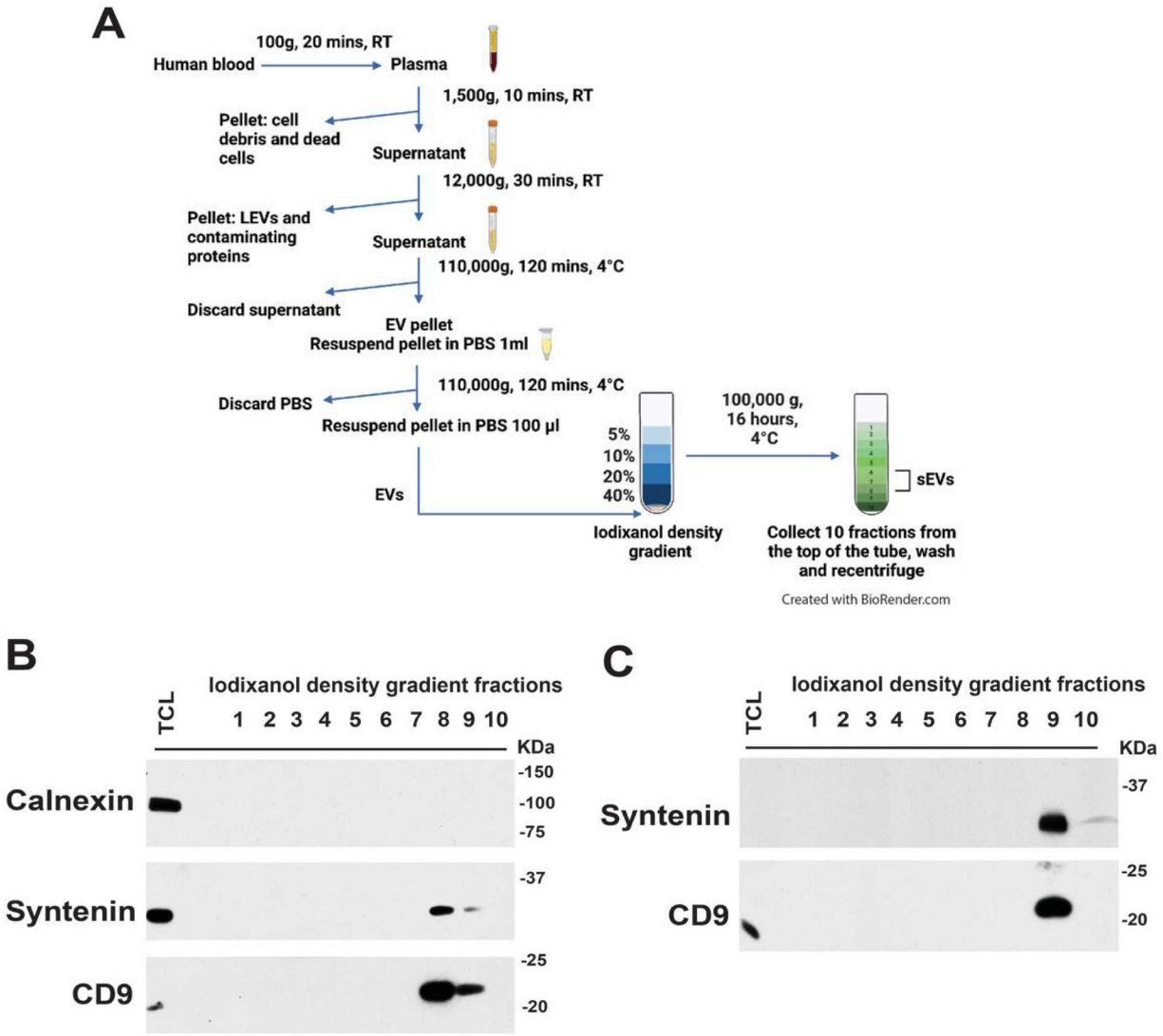

Fig. 3.

Schematic diagram showing the procedure for isolation and characterization of small extracellular vesicles from human plasma. (**A**) 20–40 ml of blood were spun at 100 × g for 20 min at room temperature (RT) to isolate plasma. In the first step, plasma was centrifuged at 1500 × g for 10 min at RT to separate supernatant from cell debris and dead cells. The collected supernatant was spun at 12,000 × g for 30 min at RT to pellet down large EVs (LEVs) and contaminating proteins. The collected supernatant was spun at 110,000 × g for 120 min at 4 °C. The resulting pellet was washed in PBS and centrifuged at 110,000 × g for 120 min at 4 °C to remove contaminating proteins. The final EV pellet was resuspended in PBS and further isolated via ultracentrifugation on IDG (40 %, 20 %, 10 %, 5% wt/vol). Following a 100,000 × g spin at 4 °C for 16 h, ten fractions were collected, washed in PBS and spun at 100,000 × g for 120 min at 4 °C. The final sEV pellet was resuspended in PBS and was biochemically and functionally characterized. (**B**) IB characterization of lysates from density gradient-isolated sEVs in fractions one to ten obtained from plasma of healthy donor A. The expression of sEV markers Syntenin and CD9 (reducing conditions)

is shown. PC3 total cell lysate (TCL) was used as a positive control for Calnexin. (**C**) IB characterization of lysates from density gradient-isolated sEVs in fractions one to ten obtained from plasma of healthy donor B. The expression of sEV markers Syntenin and CD9 (reducing conditions) is shown. PC3 total cell lysate (TCL).

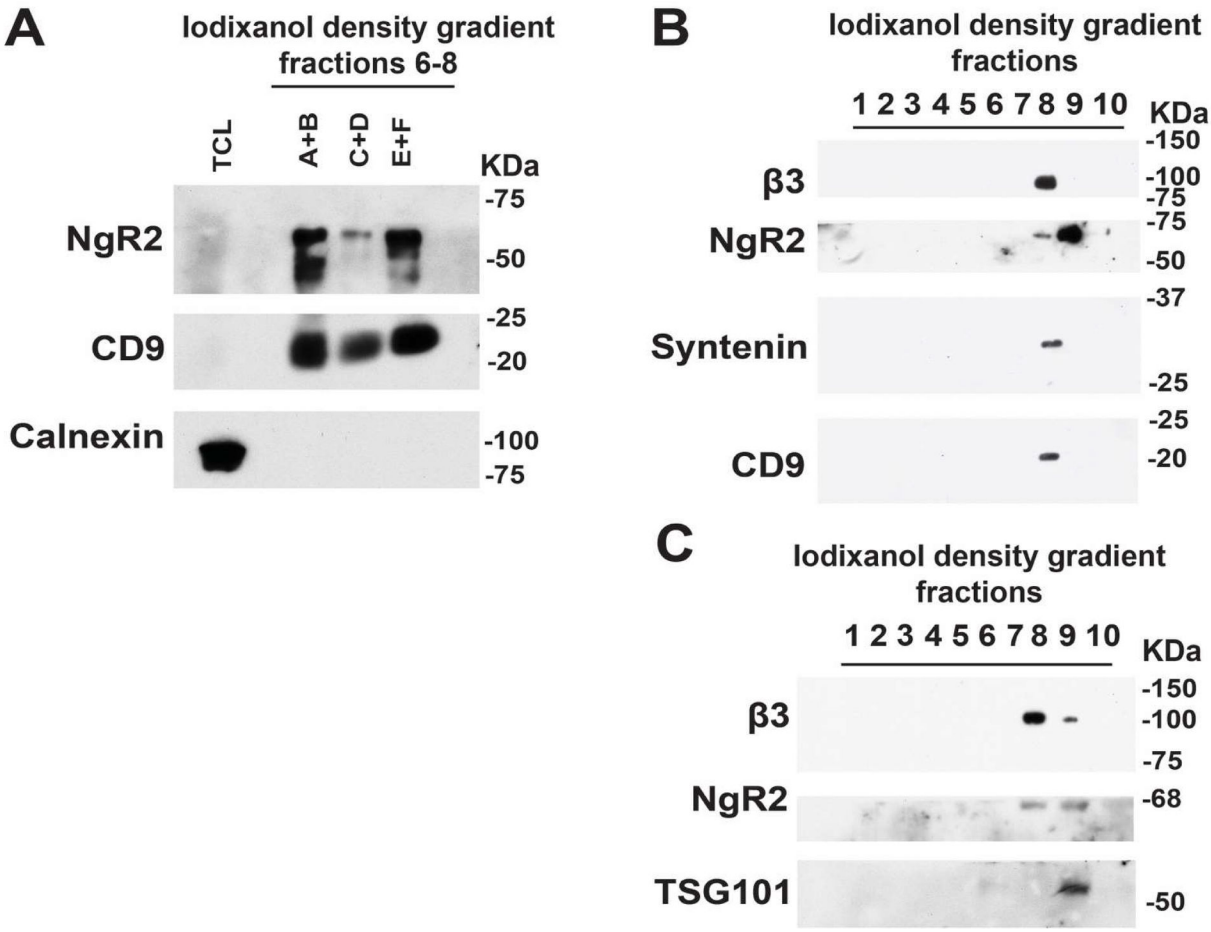

Fig. 4.

IB analysis of prostate cancer patient-derived small extracellular vesicles. (**A**) Lysates from density gradient-isolated sEVs from plasma of the following PrCa patients: A, B, C, D, E and F. Fractions six to eight were pooled and preparations from two different patients were combined. IB analysis (reducing conditions) for expression of NgR2 and CD9. PC3 total cell lysate (TCL) was used as a positive control for Calnexin. (**B**) Lysates from density gradient-isolated sEVs in fractions one to ten obtained from plasma of PrCa patient G. IB analysis (reducing conditions) for expression of αVβ3 integrin, NgR2, Syntenin and CD9. (**C**) Lysates from density gradient-isolated sEVs in fractions one to ten obtained from plasma of PrCa patient H. IB analysis (reducing conditions) for expression of αVβ3 integrin, NgR2 and TSG101.

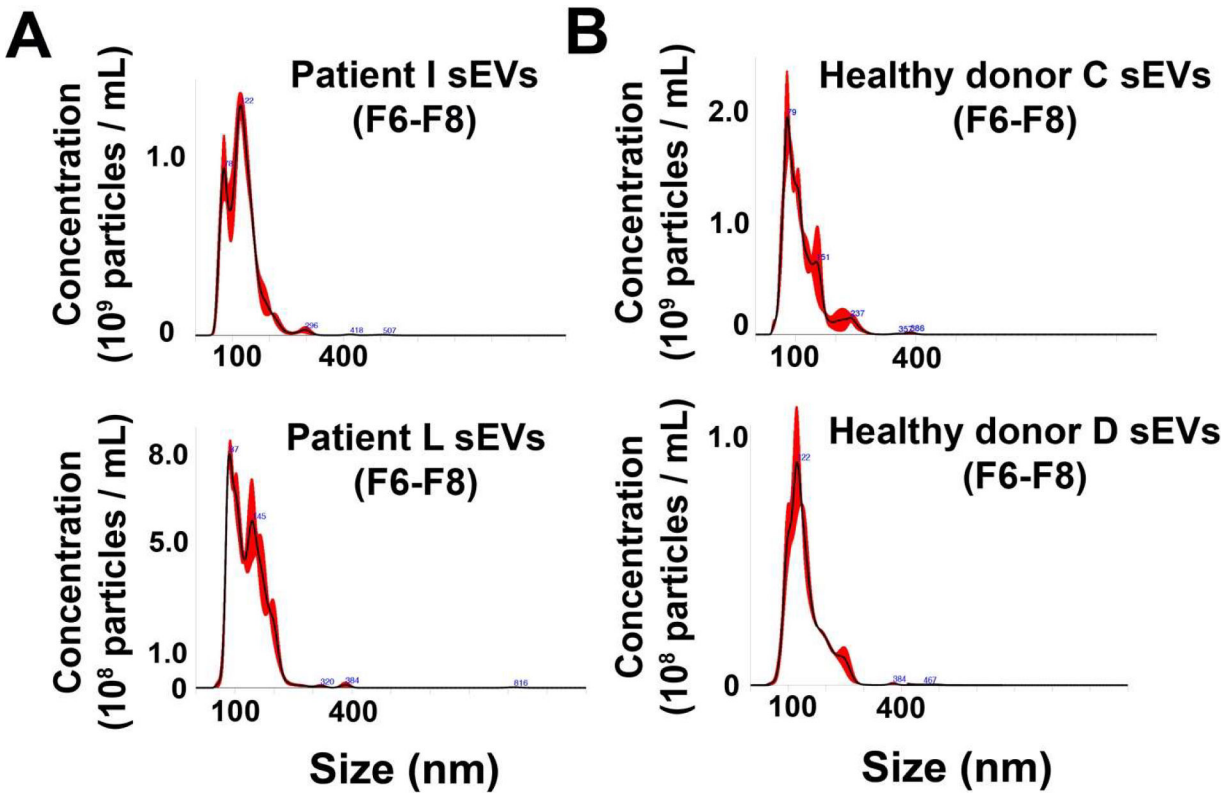

Fig. 5.

NTA characterization of prostate cancer patient- and healthy donor-derived small extracellular vesicles. (**A**) NTA of patient I and L plasma-derived, density gradient-isolated sEVs. Fractions' number six to eight were pooled (F6-F8). (**B**) NTA of healthy donor C and D plasma-derived, density gradient-isolated sEVs. Fractions' number six to eight were pooled (F6-F8).

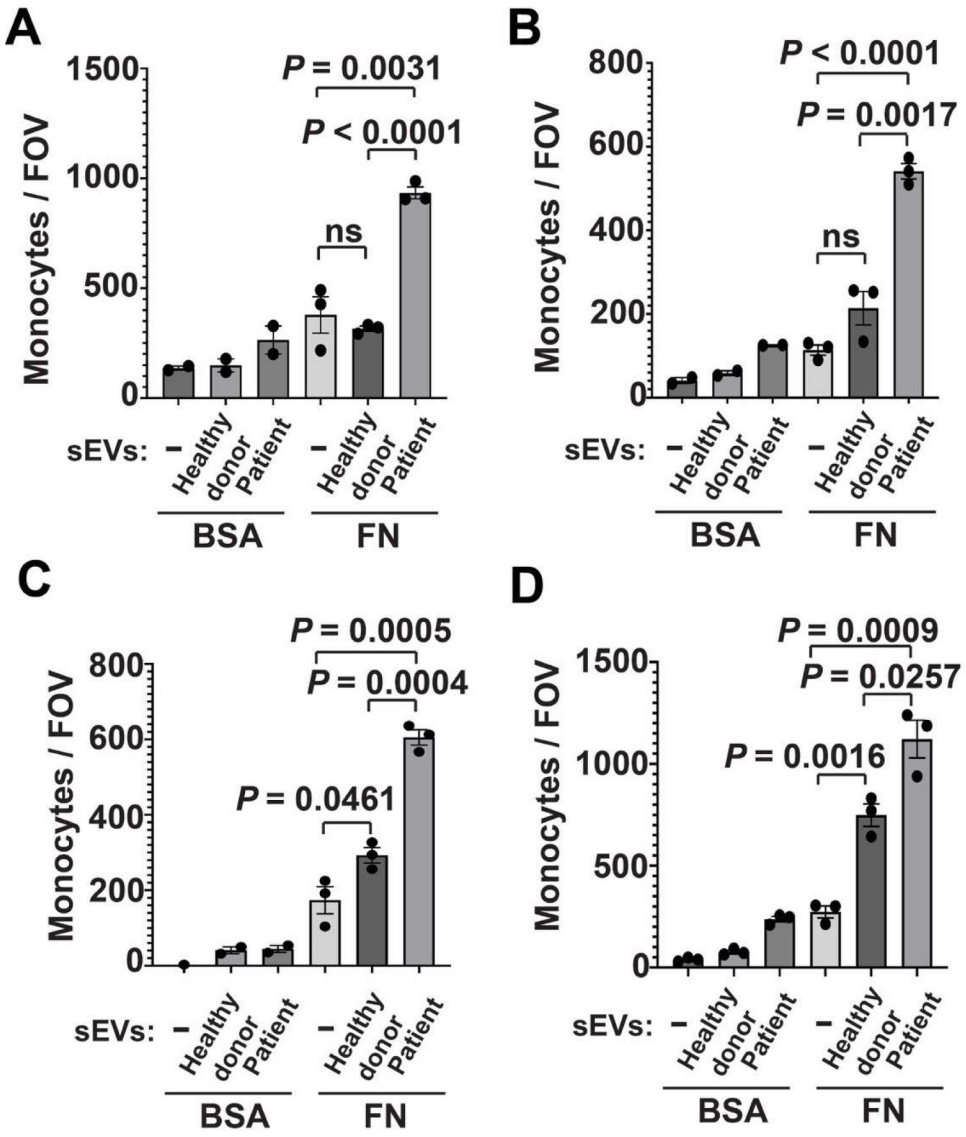

Fig. 6.

sEVs from prostate cancer patient plasma promote monocyte adhesion to fibronectin. (**A–D**) PBMCs were plated, and after 24 h they were incubated with either PBS (control), healthy donor plasma-derived sEVs, or PrCa patient plasma-derived sEVs. After 48 h, monocytes attached to wells were isolated and seeded (2.5×10^5 cells/well, 3 replicates per condition) on wells pre-coated with fibronectin (FN) (10 μg/mL) or 1 % BSA (control). A, B, C and D show four representative experiments using PBMCs from four different volunteers. Three different fields of view (FOV) were captured for each well (FOV = 0.044 mm diameter) and the number of cells for each field was counted manually on a 164×123 mm image. The values are presented as mean ± SEM; P values were calculated using *t*-test ($n = 4$).

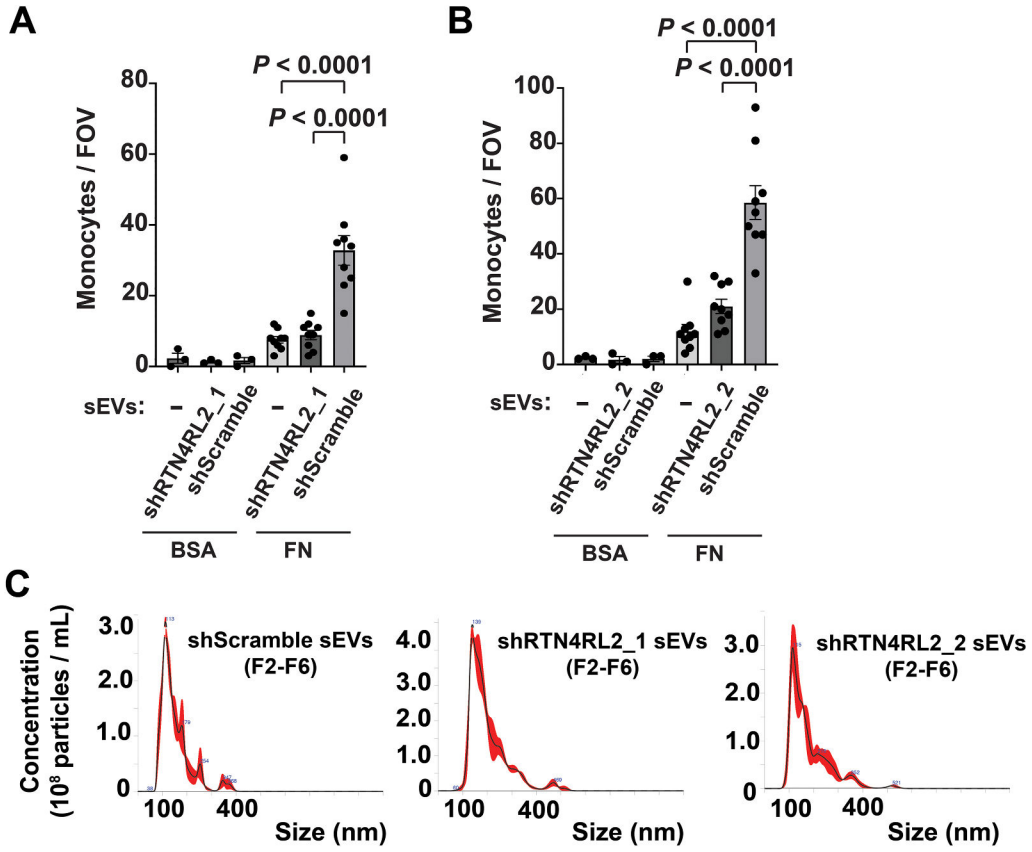

Fig. 7.

sEVs from prostate cancer cells expressing NgR2 promote monocyte adhesion to fibronectin. (**A**-**B**) PBMCs were plated and after 24 h were incubated with sEVs derived from PC3 cells transfected with NgR2 shRNA (shRTN4RL2_1 and shRTN4RL2_2), or with a non-targeting scrambled control shRNA (shScramble); untreated cells were used as a control. After 48 h, monocytes attached to wells were isolated and seeded (2.5–3 × 10^5 cells/well, 3 replicates per condition) on wells pre-coated with fibronectin (FN, 10 μg/mL) or 1 % BSA (control). A and B show two representative experiments using PBMCs from two different volunteers. Three different FOV were captured for each well (FOV = 0.044 mm diameter), and the number of cells for each field was counted manually on a 164×123 mm image. The values are presented as mean ± SEM; P values were calculated using *t*-test ($n = 3$). (**C**) NTA of shScramble (left panel), shRTN4RL2_1 (NgR2, middle panel) and shRTN4RL2_2 (NgR2, right panel) PC3 cell-derived sEVs. Fractions' number two to six were pooled (F2-F6).

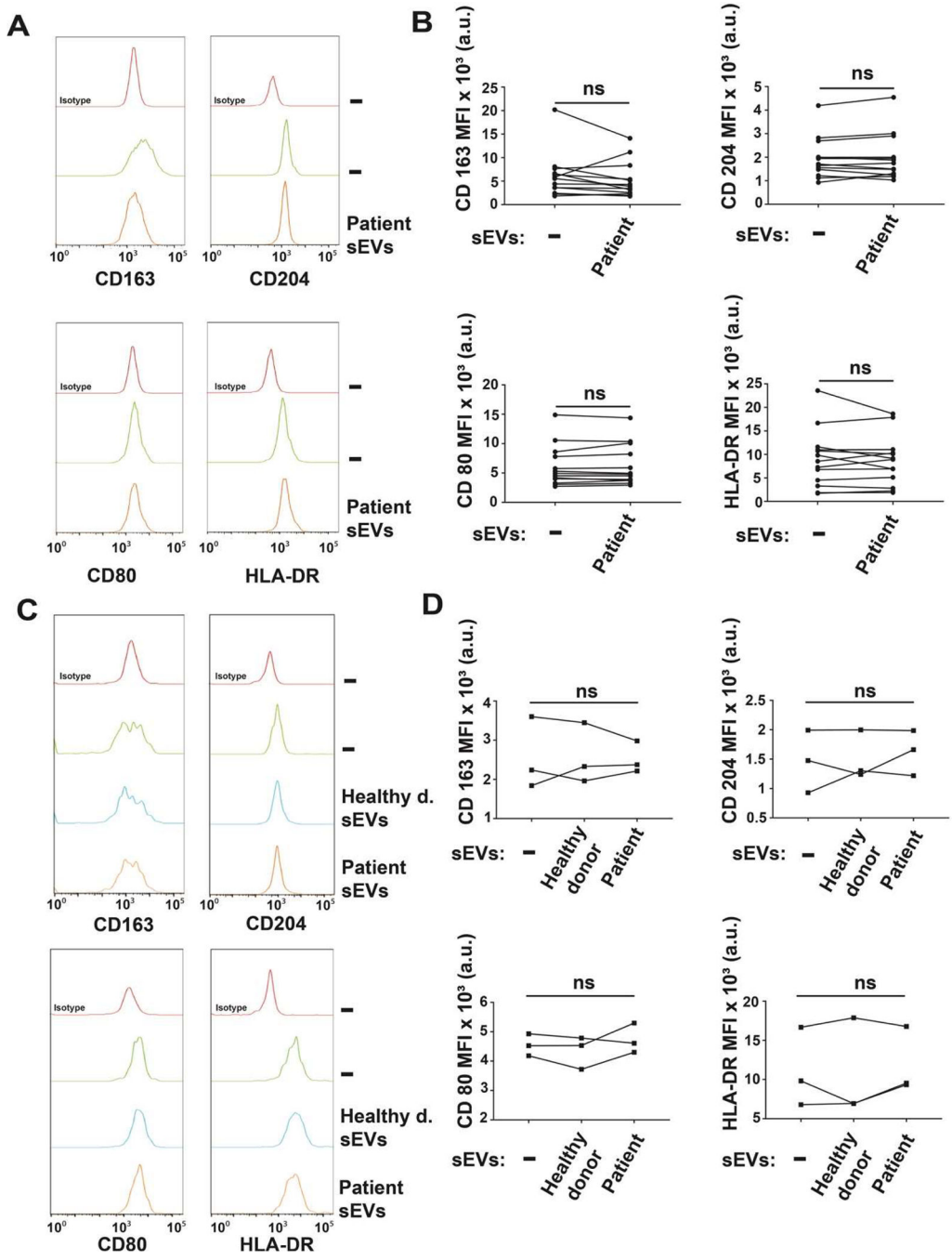

Fig. 8.

M1 and M2 marker expression is not affected by incubation with sEVs derived from healthy donors or PrCa patients. Flow cytometric analysis of monocytes isolated from healthy volunteers. (**A**) Histogram representation of the mean fluorescent intensity (MFI) of M2 polarization markers (CD163 and CD204, top panels) and M1 polarization markers (CD80 and HLA-DR, bottom panels) expressed by monocytes after incubation with PBS (−, green) or PrCa patient plasma-derived sEVs (orange) ($n = 13$). The isotype control is depicted in red. (**B**) Statistical analysis of M2 marker (CD163 and CD204, top panels) and M1 marker

(CD80 and HLA-DR, bottom panels) expression in monocytes after incubation with PBS (−) or PrCa patient plasma-derived sEVs ($n = 13$). (**C**) Histogram representation of the MFI of M2 (top panels) and M1 (bottom panels) markers expressed by monocytes after incubation with PBS (−, green), healthy donor (Healthy d.) plasma-derived sEVs (blue), or PrCa patient plasma-derived sEVs (orange) ($n = 3$). The isotype control is depicted in red. (**D**) Statistical analysis of M2 (top panels) and M1 (bottom panels) marker levels in monocytes after incubation with PBS (−), healthy donor plasma-derived sEVs or PrCa patient plasma-derived sEVs ($n = 3$). (**B, D**) The results are shown in scatter graphs. Paired *t*-test was used for paired two group comparison; ANOVA for repeated measures with Tukey's multiple comparisons test was used for multiple groups comparisons with matched samples. SAS 9.4 and Prism 7 were used for data analysis. A.U.: Arbitrary Units.

Table 1

Estimated geometric mean ratios by group - LuCaP 145.2.

Group	GMR (multiplicative growth per day)	GMR 95 % CI
IgG	1.140	(1.119,1.160)
LM609	1.038	(1.020,1.057)
PBS	1.136	(1.115,1.156)

Table 2

Pairwise comparisons of groups – tumor growth rates - LuCaP 145.2.

Comparison	Bonferroni adjusted p-value
IgG vs. PBS	1.0
LM609 vs. PBS	<0.0001
IgG vs. LM609	<0.0001

Table 3

Estimated geometric mean ratios by group – LuCaP 173.1.

Group	GMR (multiplicative growth per day)	GMR 95 % CI
IgG	1.146	(1.128,1.164)
LM609	1.045	(1.045,1.061)
PBS	1.142	(1.123,1.160)

Table 4

Pairwise comparisons of groups – tumor growth rates – LuCaP 173.1.

Comparison	Bonferroni adjusted p-value
IgG vs. PBS	1.0
LM609 vs. PBS	<0.0001
IgG vs. LM609	<0.0001